Pharmacokinetics, Toxicity, and Functional Studies of the Selective Kv1.3 Channel Blocker 5-(4-Phenoxybutoxy)Psoralen in Rhesus Macaques

L. E. Pereira,* F. Villinger,* H. Wulff,† A. Sankaranarayanan,† G. Raman,† and A. A. Ansari*,[1]

*Department of Pathology & Lab Medicine, Emory University School of Medicine, Atlanta, Georgia 30322; and †Department of Medical Pharmacology, University of California–Davis, Genome & Biomedical Sciences Facility, Davis, California 95616

The small molecule 5-(4-phenoxybutoxy)psoralen (PAP-1) is a selective blocker of the voltage-gated potassium channel Kv1.3 that is highly expressed in cell membranes of activated effector memory T cells (TEMs). The blockade of Kv1.3 results in membrane depolarization and inhibition of TEM proliferation and function. In this study, the *in vitro* effects of PAP-1 on T cells and the *in vivo* toxicity and pharmacokinetics (PK) were examined in rhesus macaques (RM) with the ultimate aim of utilizing PAP-1 to define the role of TEMs in RM infected with simian immunodeficiency virus (SIV). Electrophysiologic studies on T cells in RM revealed a Kv1.3 expression pattern similar to that in human T cells. Thus, PAP-1 effectively suppressed TEM proliferation in RM. When administered intravenously, PAP-1 showed a half-life of 6.4 hrs; the volume of distribution suggested extensive distribution into extravascular compartments. When orally administered, PAP-1 was efficiently absorbed. Plasma concentrations in RM undergoing a 30-day, chronic dosing study indicated that PAP-1 levels suppressive to TEMs *in vitro* can be achieved and maintained *in vivo* at a nontoxic dose. PAP-1 selectively inhibited the TEM function *in vivo,* as indicated by a modest reactivation of cytomegalovirus (CMV) replication. Immunization of these chronically treated RM with the live influenza A/PR8 (flu) virus suggested that the development of an *in vivo,* flu-specific, central memory response was unaffected by PAP-1. These RM remained disease-free during the entire course of the PAP-1 study. Collectively, these data provide a rational basis for future studies with PAP-1 in SIV-infected RM. Exp Biol Med 232:1338–1354, 2007

Key words: effector memory T-cells; SIV; PAP-1; K+ channel blockers.

Introduction

Voltage-gated potassium channels (Kv) regulate several physiologic functions of lymphocytes, including membrane potassium permeability, calcium influx, cytokine production, clonal expansion, and cell death (1–4). Although Kv1.3 is found in all T- and B-cell subsets in the resting state, the expression is markedly upregulated in activated effector memory T cells (TEMs) and in Ig-class–switched memory B cells, in which they increase from approximately 250 to 1500 channels per cell (5, 6). Naive T cells, central memory T cells (TCMs), and IgD^+ B cells, in contrast, increase the expression of another potassium channel, the calcium-activated channel KCa3.1, upon cellular activation (1). This differential expression of potassium channels provides an opportunity for selective inhibition of distinct cell subsets. Indeed, the KCa3.1-specific blocker TRAM-34 has been shown to preferentially suppress the proliferation of preactivated naive T cells, TCMs, and IgD^+ B cells, whereas Kv1.3-specific blockers suppress the proliferation of activated human TEMs but not of naive T cells or TCMs when stimulated with the anti-CD3 monoclonal antibody or antigen *in vitro* (5–8). Manipulation of Kv1.3 expression or function therefore could have therapeutic potential for the treatment of diseases in which TEMs or class-switched

This work was supported by grants RO1 27057, IR24RR16988, RR00165, and RO1 GM076063 from the National Institutes of Health.

H. Wulff is an inventor on the University of California patent claiming 5-(4-phenoxybutoxy)psoralen and related compounds for the treatment of autoimmune diseases. H. Wulff further holds founder stock in a start-up company (Airmid LLC) that is developing 5-(4-phenoxybutoxy)psoralen for the treatment of multiple sclerosis and possibly of psoriasis.

[1] To whom correspondence should be addressed at 101 Woodruff Circle, Room 2309, Department of Pathology and Lab Medicine, Emory University, Atlanta, GA 30322; E-mail: pathaaa@emory.edu

Received May 30, 2007.
Accepted June 20, 2007.

DOI: 10.3181/0705-RM-148
1535-3702/07/23210-1338$15.00

memory B cells contribute to pathogenesis. In proof of this hypothesis, recent studies focusing on TEM-mediated autoimmune diseases have shown that Kv1.3-specific peptides, such as ShK and its derivative ShK(L5), effectively relieve experimental autoimmune encephalomyelitis and pristane-induced arthritis in rats (9–11). However, because peptides administered *in vivo* risk inducing an immune response, particularly if chronic dosing is required, it was reasoned that a nonimmunogenic, small-molecule Kv1.3 blocker, such as the recently reported 5-(4-phenoxybutoxy)psoralen (PAP-1), would be more practical.

PAP-1 is a synthetic derivative of the natural product 5-methoxypsoralen and has been shown to exhibit a 23- to 125-fold selectivity for Kv1.3 compared with other members of the Kv1 family, effectively blocking Kv1.3 with a 50% effective concentration (EC_{50}) of 2 n*M* and a stoichiometry of two inhibitor molecules per channel (7). PAP-1 has been shown to inhibit the *in vitro* proliferation of human $CCR7^-$ TEMs significantly more potently than the proliferation of naive T cells and TCMs and to effectively suppress delayed-type hypersensitivity (DTH) in rats, a response that is mediated primarily by skin-homing $CD4^+$ TEMs (7). In addition, PAP-1 delayed diabetes onset and reduced diabetes incidence in spontaneously diabetic BB/Worchester rats at doses that did not exhibit any toxicity (11). Thus, the selective effect of PAP-1 for TEMs does not limit its application to only autoimmune diseases but also provides the potential for the treatment of other ailments in which TEMs play a major pathogenic role.

Activated memory $CD4^+$ T cells have been shown to be the primary targets for human immunodeficiency virus (HIV)/simian immunodeficiency virus (SIV) infection, which results in chronic T-cell hyperactivation that contributes to $CD4^+$ T-cell apoptosis, early immune dysfunction, and eventual exhaustion of the virus-specific immune response, ultimately leading to disease and death (12–17). These antigen-specific, memory $CD4^+$ T cells are theoretically derived from antigen-activated, naive T cells that differentiate into central and effector T cells (18, 19). SIV infection of nonhuman primates such as rhesus macaques (RM; *Macaca mulatta)* cause a disease course remarkably similar to HIV-1 infection of humans (13, 20), making this species an ideal model for the study of the effect of PAP-1 on SIV pathogenesis and to determine its potential to alter viral replication and disease course *in vivo*. The hypothesis is whether the administration of PAP-1 in SIV-infected RM prevents or slows disease progression by limiting the expansion of activated memory viral target cells and/or by contributing to the muting of the chronic immune activation response via inhibition of TEM function. Conversely, the suppression of a virus-specific, effector T-cell response could also have detrimental effects on the control of viral replication and may accelerate the course of infection. Thus, investigating the influence of PAP-1 on SIV pathogenesis will help define cell lineages and/or mechanisms that are involved in the protection or deterioration of the immune system following SIV infection in this species. Before such a task is undertaken, it is vital to first assess both the *in vitro* and *in vivo* effects of PAP-1 in RM. The goal of this study was to determine the potential toxicity, if any, and the pharmacokinetics (PK) of PAP-1 in healthy, uninfected RM in order to determine a therapeutic dose of PAP-1 that could be used in SIV-infected animals in the future. A single dose of PAP-1 was initially administered to RM and, upon determination of the safety and PK, a chronic dosing study was initiated to determine the dosage required to maintain a critical trough level of this compound. RM undergoing chronic PAP-1 dosing were also infected intranasally with a live attenuated influenza A/PR8 (flu) virus and the effect of PAP-1 on the primary effector and the secondary memory flu-specific responses were assessed in order to confirm the target-cell selectivity of PAP-1 *in vivo*. In parallel with these *in vivo* studies, *in vitro* experiments were performed to define the Kv1.3 channel expression profile in T-cell subsets in RM and to determine the potential *in vitro* suppressive effect of PAP-1 on activated TEMs in RM. Results suggest that PAP-1 was both safe and effective *in vitro* and *in vivo*, which provides a rational and sound foundation for future studies with PAP-1 in SIV-infected RM.

Materials and Methods

Animals. Healthy, SIV-negative RM of comparable age and weight were housed at the Yerkes National Primate Research Center of Emory University. Their housing, care, diet, and maintenance were in conformance to the guidelines of the Committee on the Care and Use of Laboratory Animals of the Institute of Laboratory Animal Resources, National Research Council and of the Health and Human Services by the standard guidelines, "Guide for the Care and Use of Laboratory Animals" (21). RM were anesthesized with 10 mg/kg of ketamine hydrochloride that was administered intramuscularly. For acute PAP-1 dosing experiments that required multiple bleeds at frequent time intervals, anesthesia was administered every 2–4 hrs as needed. On days when only a single bleed was required, a single dose of ketamine was administered prior to sample retrieval. RM that were immunized with the flu virus for the chronic dosing study were anesthesized and were intranasally administered 1 ml of solution that contained 1024 hemagglutinin antigen (HA) units of the virus in a slow, drop-by-drop fashion, as described elsewhere (22). The animals were also boosted 4 weeks and 12 weeks after the initial immunization with the same viral dose and by the same route of administration.

PAP-1. PAP-1 was synthesized as previously described (7). For the *in vitro* assays, PAP-1 was dissolved in dimethylsulfoxide (DMSO) to a concentration of 10 m*M*, and this stock solution was diluted to desired concentrations using RPMI-1640 medium that was supplemented with 1% fetal calf serum (FCS), 2 m*M* glutamine, and 50 μg/ml gentamycin. The final DMSO concentration in the culture

assays was ≤0.05%. For intravenous administration, PAP-1 was dissolved at a concentration of 9 mg/ml in a mixture of cremophor (Sigma-Aldrich, St. Louis, MO) and 1× phosphate-buffered saline (PBS; 1:4) by heating to approximately 90°C and then vigorously stirring. Aliquots of the cooled PAP-1 solution were frozen at –20°C until use. For oral administration, PAP-1 was mixed at a final dosage of 25 mg/kg for each animal into approximately 5 g of chocolate paste just prior to administration and the stock was stored at 4°C for no more than a week before being fed to the animals.

Specimen Collection and Toxicity Analyses. Whole blood was collected from the RM in heparinized tubes for the determination of absolute counts of white blood cells (WBCs), platelets, and the total lymphocyte count using standard methods. In addition, sera were evaluated for the levels of albumin, liver enzymes, bilirubin, blood urea nitrogen/creatinine, and various electrolytes, using our standard *in vivo* toxicology screen. Peripheral blood mononuclear cells (PBMCs) were also isolated from heparinized whole blood by standard Ficoll-Hypaque gradient centrifugation.

Determination of Plasma PAP-1 Levels by High-Performance Liquid Chromatography (HPLC)-Mass Spectroscopy. PAP-1 was injected intravenously or was administered orally to two rhesus macaques (12 and 17 kg, respectively). At various time points following administration, approximately 0.5 ml of blood was collected into EDTA–blood sample collection tubes. Plasma was separated by centrifugation and was stored at –20°C, pending analysis. Samples were purified using C18, solid-phase extraction (SPE) cartridges. Elution fractions corresponding to PAP-1 were evaporated to dryness under nitrogen and were reconstituted in a 2:3 mixture of acetonitrile (ACN) and water. Liquid chromatography electrospray ionization tandem mass spectrometry analysis was performed with a Hewlett-Packard 1100 series HPLC stack that was equipped with a KGaA RT 250-4 LiChrosorb RP-18 column (Merck, Darmstadt, Germany) and an HP 1100 variable-wavelength detector (VWD) and was interfaced to a Finnigan LCQ Classic Mass Spectrometer (MS; Thermo Fisher Scientific, Waltham, MA). The mobile phase consisted of ACN:H_2O with 0.2% formic acid. The flow rate was 1.0 ml/min, and the gradient was ramped from 1:1 to 9:1 ACN:H_2O over 20 mins. While the column temperature was maintained at 24°C, PAP-1 was eluted at 14.8 mins and was detected with the VWD and the MS in series. Quantitation was performed by electrospray ionization MS/MS (capillary temperature = 350°C; capillary voltage = 5 V; tube-lens offset = –25 V; positive-ion mode; normalized collision energy = 25.7%; parent mass = 351.1 m/z; SRM = 107.0, 149.0, 251.0, 351.2) for samples between 2.5 n*M* (0.88 ng/mL) and 750 nm (263 ng/mL) and by the VWD (310 nm) for samples with higher concentrations. The related compound 5(4-phenoxypropoxy)psoralen (PAP-3; formula weight = 336.33; RT = 13.5 mins) was used as an internal standard. The pharmacokinetics of the data obtained on samples following intravenous injection were plotted as a two-compartment model, using both Origin (Rockware Inc., Golden, CO) and Winnonlin software (Pharsight, Mountain View, CA).

Flow Cytometry Analysis. Aliquots of the PBMCs were subjected to standard immunophenotypic analysis to determine the frequencies of major T-cell subsets, including naive cells, TCMs, TEMs, and regulatory T-cells (Tregs), using the following antibody clones: CD4-PerCP (clone L200), CD8-FITC (clone SK1), CD28-PE (clone 28.2), and CD95-APC or -FITC (clone DX-2), all purchased from BD Pharmingen (San Diego, CA); CD25-PE (clone 4E3; Miltenyi Biotec, Auburn, CA); and FoxP3-APC (clone PCH101; eBioscience, San Diego, CA). To phenotype-naive, TCM, and TEM subsets, cells were first incubated with 1 μg/ml of anti-FcR antibody (clone 2.4G2; courtesy of Dr. R. Mittler, Emory University Center for AIDS Research) for 15 mins at 4°C, were washed, and then were surface-stained for 15 mins at 4°C with predetermined optimal concentrations of CD4-PerCP, CD8-FITC, CD28-PE, and CD95-APC. Cells were washed, resuspended in freshly prepared 1% paraformaldehyde in PBS (pH 7.4) and were analyzed. T-cell subsets were defined as naive ($CD28^+CD95^-$), TCM ($CD28^+CD95^+$), and TEM ($CD28^-CD95^+$; Ref. 23). In the Treg phenotypes, cells were surface-stained in a similar manner, using CD4-PerCP and CD25-PE. Fixation and intracellular staining to detect FoxP3 were performed according to eBioscience protocol. Appropriate monoclonal antibody–isotype controls were included. Flow-cytometric acquisition of at least 100,000 total events from each sample was performed on a FACS Calibur flow cytometer (BD Biosciences, San Jose, CA). Data acquisition and analysis were performed using CellQuest (BD Biosciences) and FlowJo (TreeStar, Ashland, OR) software, respectively.

Proliferation Assays. PBMCs were isolated from the peripheral blood of healthy RM ($n = 9$) and were resuspended in RPMI at a concentration of 1,000,000 cells/ml. One hundred microliters of solution that contained 100,000 cells were dispensed into each well of a 96-well polystyrene plate that was previously coated overnight with 400 ng/ml of anti-CD3 monoclonal antibody (clone FN-18; Biosource, Invitrogen, Carlsbad, California). PAP-1 was added in a volume of 100 μl of RPMI at increasing concentrations. Cultures were performed in triplicate. For the isolation of $CD28^-$ effector memory cells, PBMCs were incubated with anti-CD28–coated magnetic beads (Dynal Cellection Kit; Invitrogen) for 30 mins at 4°C with gentle rotation. $CD28^+$ cells bound to the beads were separated (5 mins × 2) using a magnet, and the supernatant containing $CD28^-$ cells was washed twice with 1% RPMI. An aliquot of these isolated cells was subjected to flow analysis, and the purity of the $CD28^-$ cell population was always greater than 90%. The negatively isolated CD28-fraction was seeded at 100,000 cells/well in the absence or presence of

increasing concentrations of PAP-1. Cultures were incubated at 37°C and 7% CO_2 for 3 days, and cells were pulsed with [^{3}H]-thymidine (1 μCi/well) at 16 hrs prior to harvest. Cells were harvested onto glass-fiber filters, and the mean uptake of [^{3}H]-thymidine was determined using a standard β-scintillation counter.

Electrophysiology. Electrophysiologic studies were conducted on aliquots of both resting and *in vitro* activated, unfractionated and fractionated T-cell subsets. The T cells were isolated from PBMCs by negative selection, using an RM-specific T-cell enrichment kit (StemCell Technologies Inc., Vancouver, Canada). Aliquots of the isolated T cells were activated with 10 μg/ml of plate-bound anti-CD3 (clone FN-18; BioSource/Invitrogen) for approximately 40 hrs. Both resting and *in vitro,* activated T cells were stained for CD28 and CD95 on ice in an RPMI medium (supplemented with 10% FCS and 0.1% NaN_3) with phosphatidylethanolamine (PE)-conjugated mouse anti-human CD28 monoclnal antibody (CD28.2; BD Pharmingen) and FITC-conjugated mouse antihuman CD95 monoclonal antibody (DX2; BD Pharmingen). Cells were washed, were incubated on poly-L-lysine–coated coverslips, and were kept in the dark at 4°C for 10–30 mins to allow attachment. Naive cells ($CD28^+CD95^-$), TCMs ($CD28^+CD95^+$), and TEMs ($CD28^-CD95^+$) were visualized by fluorescence microscopy and were studied in the whole-cell configuration of the patch-clamp technique.

Kv1.3 currents were elicited *in situ* by repeated 200-ms pulses from a holding potential of −80 mV to 40 mV, which were applied either every second to visualize the characteristic cumulative inactivation of Kv1.3, or every 30 secs in experiments to measure the blocking activity by ShK(L5) or PAP-1 on Kv1.3 currents. Currents were recorded in normal Ringer's solution with a calcium-free pipette solution that contained the following: 145 m*M* KF, 10 m*M* HEPES, 10 m*M* EGTA, and 2 m*M* $MgCl_2$ (pH 7.2; 300 mOsm). Whole-cell Kv1.3 conductance measurements were calculated from the peak current amplitudes at 40 mV. KCa3.1 currents were elicited with voltage ramps from −120 mV to 40 mV of 200 msecs duration, which were applied every 10 secs with a pipette solution containing the following: 145 m*M* potassium aspartate, 2 m*M* $MgCl_2$, 10 m*M* HEPES, 10 m*M* K_2-EGTA, and 8.5 m*M* $CaCl_2$ (1 μ*M* free calcium; pH 7.2; 290 mOsm). To reduce chloride leak currents, we used a sodium aspartate, external solution containing the following: 160 m*M* sodium aspartate, 4.5 m*M* KCl, 2 m*M* $CaCl_2$, 1 m*M* $MgCl_2$, and 5 m*M* HEPES (pH 7.4; 300 mOsm). Kv1.3 and KCa3.1 channel numbers per cell were determined by dividing the whole-cell Kv1.3 or KCa3.1 conductance by the single-channel conductance value for each channel—Kv1.3: 12 pS; IKCa1: 11 pS. Cell capacitance, a direct measure of cell surface area, was constantly monitored during recording. Resting (unstimulated) T cells had membrane capacitances less than 2 pF (average cell diameter < 7 μm), whereas activated cells had membrane capacitances greater than 4 pF (average cell diameter > 11 μm).

Real-Time Polymerase Chain Reaction (PCR) for Rhesus Cytomegalovirus (RhCMV) Quantification. A real-time PCR assay was performed to quantify RhCMV DNA copy numbers in plasma samples from the RM undergoing the PAP-1 chronic dosing study by measuring levels of the pp65 virus sequence. The template for the reaction was total viral DNA, isolated from the plasma samples using the QIAamp DNA Mini Kit (Qiagen, Valencia, CA). Each plasma sample was spiked with an equal amount (10,000 copies) of an unrelated plasmid that contained the chloramphenicol acetyl transferase (CAT) sequence to control for the efficiency of DNA extraction. These were later subjected to and were quantified by PCR using CAT-specific primers, as described before (24, 25), to serve as an internal control by confirming uniformity in DNA isolation from each plasma sample. The forward primer (5′-GTTTAGGGAACCGCCATTCTG-3′) corresponded to residues 719–739, and the reverse primer (5′-GTATCCGCGTTCCAATGCA-3′) corresponded to residues 826–808 (26). Reactions of a 20-μl total volume containing 1× iQ SYBR Green Supermix (BioRad), 100 ng/μl of each primer, nuclease-free water, and the template from each plasma sample were prepared in duplicate. PCR was performed on an iCycler (BioRad, Hercules, CA) under the following conditions: 10 mins at 95°C followed by 45 cycles of 15 secs at 95°C and of 1 min at 60°C. A standard curve was generated by using 10-fold serial dilutions of a control, pGEM-T plasmid containing the pp65 target sequence (10^6–0 copies per reaction). Results were analyzed using the iCycler iQ Optical System software (BioRad), and the limit of sensitivity was reproducibly between 1–10 copies of the template.

Determination of Flu-Specific, Cell-Mediated, and Humoral Responses. For determination of $CD4^+$ and $CD8^+$ T-cell responses, aliquots of PBMCs from each monkey were cultured for 2 hrs with whole-flu virus (approximately 100 HA units/well), ConA (positive control; 7.5 μg/ml), or OVA peptide (negative control; 3 μg/ml) followed by the addition of brefeldin A (6 μg/ml) and incubation overnight at 37°C and 5% CO_2. Cells were washed and were surface-stained with CD4-PerCP and CD8-FITC (BD Pharmingen) and then were fixed/permeabilized and were stained for intracellular IFN-γ-APC or for IL2-APC and TNF-α-PE (all from BD Pharmingen). The frequency of cytokine-producing, $CD4^+$ or $CD8^+$ cells was determined by standard flow cytometric analysis on the FACS Calibur II (BD Biosciences). For determination of humoral responses, a standard enzyme-linked immunoabsorbant assay (ELISA) to detect flu-specific IgG was performed. Briefly, 96-well plates were coated with poly-L-lysine and, whole-flu virus was dispensed into individual wells overnight. The plates were washed, and media containing 2% non-fat milk solution was added for blocking non-specific binding. The 100 μl of plasma to be assayed

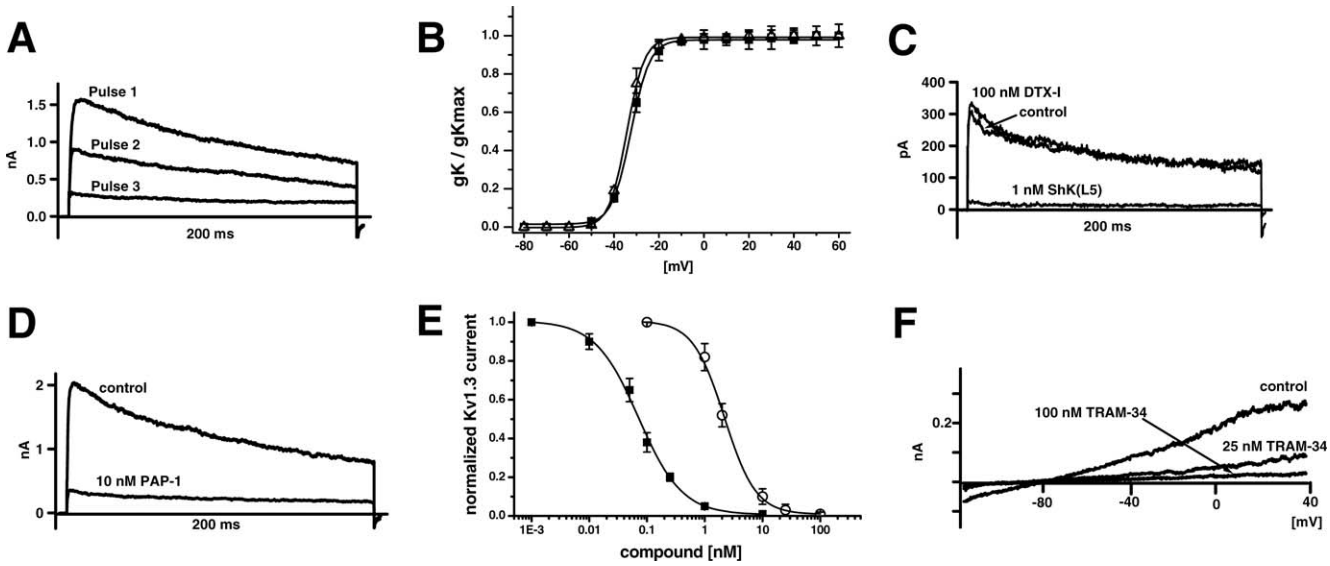

Figure 1. T cells in RM express Kv1.3 and KCa3.1. (A) The Kv current exhibits the characteristic use-dependence of Kv1.3 when currents are elicited with 200-msec pulses every 1 sec. (B) Normalized, peak potassium conductance-voltage relationship of Kv current in resting (■; $V_{1/2} = -34 \pm 1.4$ mV) and activated (△; $V_{1/2} = -33 \pm 1.2$ mV) T cells in RM (n = 3). (C) The Kv current in a naive T cell is insensitive to the Kv1.1-blocking peptide toxin DTX-I and is sensitive to the Kv1.3-specific blocker ShK(L5). (D) Blockade of the Kv current in an activated TEM by PAP-1. (E) Concentration-response curve for Kv current inhibition by ShK(L5) (■; $IC_{50} = 72 \pm 8$ p*M*; $n_H = 1.15$) and PAP-1 (○; $IC_{50} = 2.1 \pm 0.3$ n*M*; $n_H = 1.8$). (F) KCa current in a naive T cell, as elicited by dialysis with 3 μ*M* free calcium. The current is blocked by the specific KCa3.1 blocker TRAM-34. Kv1.3 was previously blocked by 1 n*M* ShK(L5).

was diluted to 1:100, 1:1000, 1:5000, 1:10000, and 1:50000 in 10% RPMI, which then were added in triplicate wells. Plates were incubated at 37°C for 2 hrs and washed four times with PBS-T. Then, 100 μl of 1:2000 diluted alkaline-phosphatase–conjugated antihuman Ig (Southern Biotech, Birmingham, AL) was added to each well. After a 1-hr incubation at 37°C, wells were washed, and the reaction was developed using an alkaline phosphatase substrate kit (BioRad, Hercules, CA). Wells were monitored for color development, and absorbance was measured at 405 nm. The cut-off value was determined as the mean of the negative control plus three times its standard deviation (SD). Samples with mean absorbance readings exceeding this value were considered positive for the presence of flu-specific IgG, and the reciprocal of the highest dilution of plasma that gave a positive reaction was considered the titer in the sample being tested.

Statistical Analyses. Data are represented as mean ± SD unless otherwise indicated. Any statistical analyses to determine significant differences were derived using the two-tailed Student's *t* test. A *P* less than 0.05 was considered statistically significant.

Results

Kv1.3 Expression in RM T Cells is Comparable to Levels Present in Human T Cells. Prior to investigating the *in vivo* and *in vitro* effects of PAP-1 in RM, it was essential to first determine if RM resemble humans and express Kv1.3 and KCa3.1 in a T-cell subset–specific manner. Because there are currently no specific antibodies to Kv1.3 or KCa3.1 suitable for use in flow cytometry, a combination of fluorescence microscopy and electrophysiology were utilized to study potassium-channel expression in RM, as was previously done in human T cells (5). $CD3^+$ lymphocytes were isolated by negative selection from PBMCs of healthy RM ($n = 6$); both resting and anti-CD3 activated T cells were stained with CD95-FITC and CD28-PE to distinguish among naive, TCM, and TEM subsets and their potassium currents were measured in the whole-cell mode of the patch-clamp technique. Each subset expressed Kv currents, which were confirmed to be Kv1.3 by their biophysical and pharmacologic properties. The currents exhibited the Kv1.3 characteristic use-dependence upon rapid pulsing, and they showed the same inactivation time constant (approximately 200 ms; Fig. 1A) and half-activation voltage ($V_{1/2} = -33$ mV; Fig. 1B) as the cloned channel (27). Furthermore, the Kv current in all three T-cell subsets was inhibited by the Kv1.3-specific blockers ShK(L5) and PAP-1, with 50% inhibitory concentrations (IC_{50}s) of 72 p*M* and 2.1 n*M*, respectively. See Figures 1C and 1D for representative recordings and Figure 1E for the concentration-response curves. The Kv1.1-specific peptide DTX-1 had no effect on the current at a concentration of 100 n*M*, demonstrating that, in contrast to mouse T cells, T cells in RM do not express functional Kv1.1 channels. See Figure 1C for a representative recording from a resting naive T cell. In addition to Kv1.3 currents, we also detected calcium-activated potassium currents that exhibited the biophysical and pharmacologic characteristics of KCa3.1 in T cells of RM when dialyzing 3 μ*M* of free calcium through the recording pipette. The currents reversed around –80 mV and

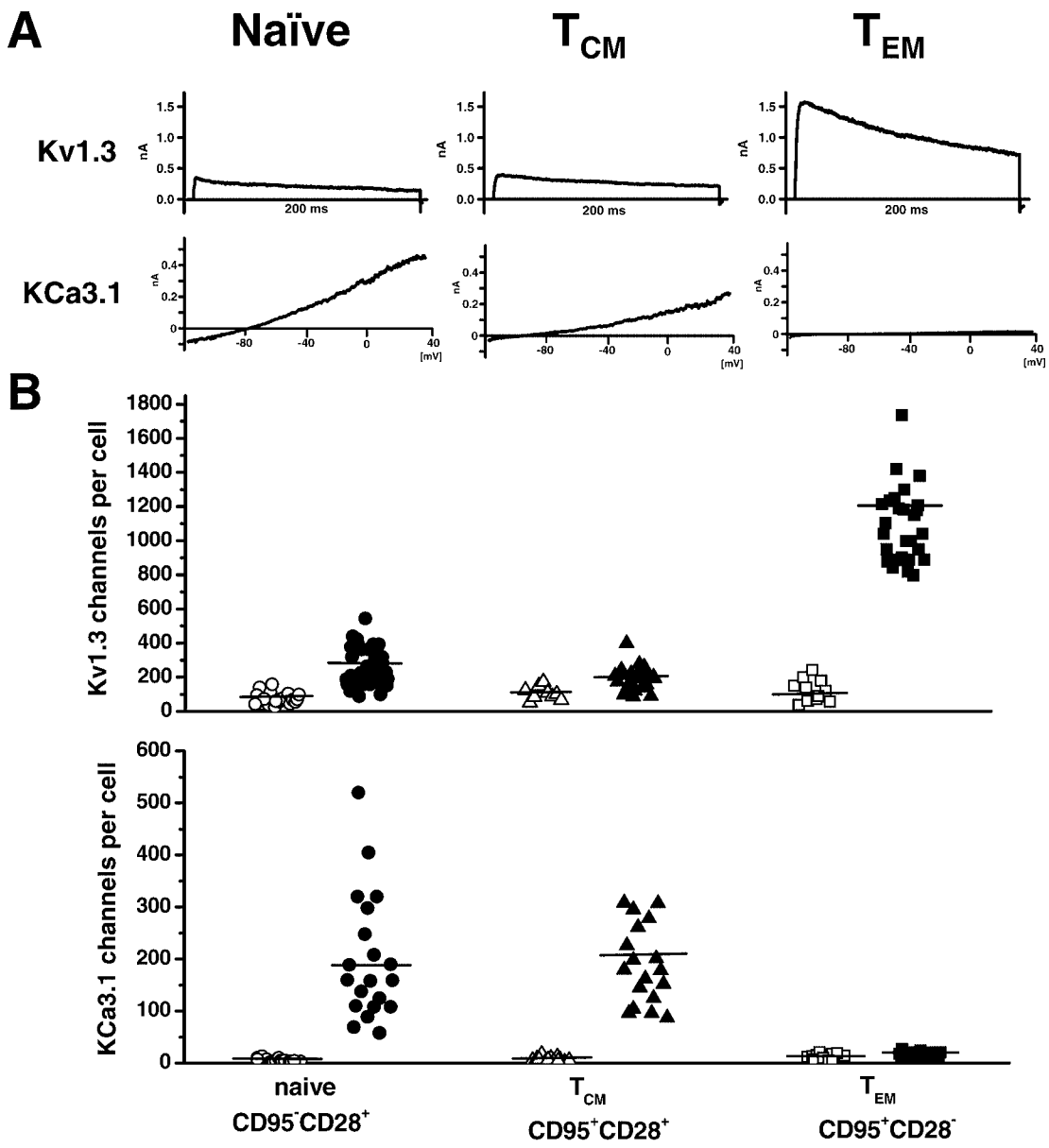

	naive		T_{CM}		T_{EM}	
	resting	activated	resting	activated	resting	activated
Kv1.3 channels/cell	74 ± 32 (n = 23)	251 ± 107 (n = 40)	105 ± 38 (n = 9)	194 ± 67 (n = 26)	123 ± 65 (n = 11)	1083 ± 217 (n = 28)
KCa3.1 channels/cell	5 ± 3 (n = 17)	199 ± 120 (n = 20)	7 ± 4 (n = 14)	189 ± 76 (n = 18)	13 ± 5 (n = 16)	16 ± 6 (n = 18)

Figure 2. (A) Representative Kv1.3 and KCa3.1 currents in activated naive cells, TCMs, and TEMs in RM. (B) Scatterplot of Kv1.3 and KCa3.1 channel numbers per cell in resting (open symbols) and activated (closed symbols) T cells in naive cells, TCMs, and TEMs in RM. Mean ± SD channel numbers are shown in the table below the plot.

were sensitive to blockade by the specific KCa3.1 blocker TRAM-34 (Fig. 1F).

In addition, the numbers of Kv1.3 and KCa3.1 channels in naive cells, in TCMs, and in TEMs were also determined by patch-clamping roughly 20 cells from each subset in both the resting and activated state and then by dividing the whole-cell Kv1.3 or KCa3.1 conductance by the single channel conductance value for each channel (see Figure 2A for representative Kv1.3 and KCa3.1 currents). Although the number of Kv1.3 channels is generally slightly lower in RM than in human T-cells (5), the expression pattern is very similar. As seen with naive cells and TCMs in humans, the upregulation of Kv1.3 channels in these cell subsets in RM was minimal upon activation; however, as anticipated, activated TEMs from RM exhibited a significant (approximately 8-fold) increase in Kv1.3 channels similar to the level

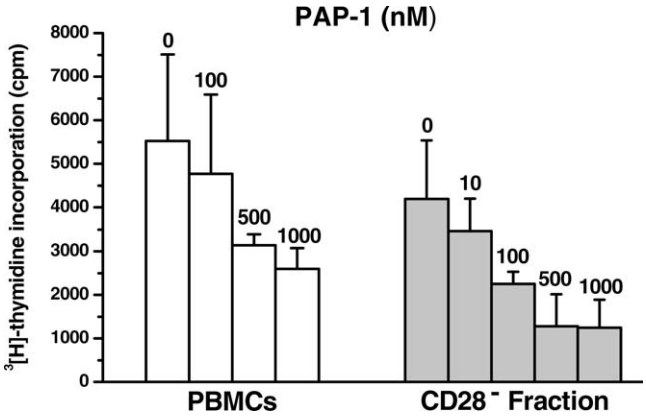

Figure 3. PAP-1 suppresses the proliferation of PBMCs and TEMs from RM. PBMCs isolated from healthy, uninfected RM ($n = 9$) were seeded at 100,000 cells/well and were stimulated with 400 ng/ml, plate-bound anti-CD3 in the absence or presence of increasing concentrations of PAP-1 (n*M*). To test the effect of PAP-1 on TEMs, PBMCs were depleted of $CD28^+$ cells using anti-CD28–coated magnetic microbeads, and the $CD28^-$ fraction was seeded at 100,000 cells/well. Cultures were incubated at 37°C and 7% CO_2 for 3 days. Cells were pulsed with 1 uCi/well [^{3}H]-thymidine at 16 hrs prior to harvest, and thymidine uptake was measured by standard scintillation counting. The mean cpm ± SD was determined; data shown is representative of three independent assays.

of upregulation that occurs in activated human TEMs. In contrast, there was an approximately 30- to 40-fold increase in the number of KCa3.1 channels in activated naive cells and TCMs, with no upregulation occurring in the TEM subset. The differential upregulation of these potassium channels among the T-cell subsets was reflected by the increase in Kv1.3 and KCa3.1 currents in activated TEM cells and in naive cells or TCMs, respectively (Fig. 2A). Staining with the CD95 and CD28 antibodies did not interfere with the expression pattern of Kv1.3 and iKCa3.1 currents (data not shown). Taken together, these data indicate that Kv1.3 and KCa3.1 are the only potassium channels expressed in T cells of RM and that their expression pattern is similar to human T cells. Although KCa3.1 is the dominating channel in activated naive cells and in TCMs, activated TEMs express a $Kv1.3^{high}$ phenotype.

PAP-1 Inhibits the Proliferation of RM PBMCs and TEM Cells *in vitro*. Recent studies demonstrated that Kv1.3 expression in human T cells is low in both $CD4^+$- and $CD8^+$-naive cells and in TCMs; expression is high in both activated $CD4^+$ and $CD8^+$ $CCR7^-$ TEMs (7). As a result, PAP-1 effectively suppressed the proliferation of human $CCR7^-$ TEMs *in vitro*, with an IC50 of 10 n*M* (7). It was reasonable to assume that the same would be true in RM, and we therefore evaluated the effect of PAP-1 on total $CD28^-$ T cells, because TEMs in RM are best defined by the $CD28^-CD95^+$ phenotype (23). Thus, to determine if a comparable degree of suppression was observed with TEMs in RM, an *in vitro* assay was performed in which $CD28^-$ TEMs were negatively isolated from PBMCs in RM ($n = 9$) using anti-CD28–coated magnetic microbeads. Negatively isolated cells were confirmed to be 90% $CD28^-$ by flow cytometry. This $CD28^-$ fraction, containing primarily the TEM subset, was stimulated *in vitro* with a low, suboptimal concentration of plate-bound anti-CD3 in order to preferentially activate TEMs, which exhibit a lower activation threshold than naive cells or TCMs (28). As shown by the representative data in Figure 3, PAP-1 suppressed the proliferation of TEMs with an IC_{50} of approximately 100 n*M*. The suppressive effect of PAP-1 on bulk PBMCs, which predominantly consist of naive cells and TCMs, was also tested and was found to be less pronounced with an IC_{50} of approximately 1 μ*M* (Fig. 3). Isolated $CD28^+$ T cells could not be utilized as a pure source of naive cells and TCMs, because the T cells still contained bound anti-CD28 antibody when released from the magnetic beads. This in combination with anti-CD3 resulted in a level of stimulation that abrogated the suppressive effect of PAP-1. This observation is in line with a previous study which reported that T cell proliferation was unaffected by the potassium channel blocker margatoxin when costimulation with anti-CD28 was involved (4). In summary, the results obtained suggest that PAP-1 is an effective inhibitor of TEM proliferation in RM, which is consistent with previous studies.

Acute *In Vivo* Dosage Studies Suggest that PAP-1 Is Non-Toxic and that Its PK Is Best Reflected by a Two-Compartment Model. To determine the *in vivo* toxicity and PK of PAP-1, two adult RM, RHg7 and RVe7, were administered the compound intravenously at a dose of 3 mg/kg. The intravenous administration of PAP-1 was well tolerated by both animals with no signs of acute side effects. Blood and serum biochemical parameters were determined at 48 hrs and at 7 days postadministration, and comparison with baseline levels suggested no evidence of PAP-1–related hematologic and organ toxicity (Table 1). An increase in the levels of serum creatinine phosphokinase (CPK) from baseline levels was observed in both RM, but this was attributed to the effect of the anesthetic ketamine hydrochloride that was used to sedate the animals for blood sample collection. Ketamine anesthesia and the physical restraint associated with its administration have been shown to induce variations in several serum and hematologic parameters in nonhuman primates, including RM and cynomologus monkeys (29, 30). Indeed, repeated ketamine administration that was necessary for multiple blood sample withdrawal within the first 48 hrs of the acute PAP-1 dosing experiment led to alterations in CPK activity and to fluctuations in other biochemical variables, such as glucose and aspartate transaminase (AST), in both RHg7 and RVe7. A decrease in circulating lymphocytes with a coincident increase in neutrophils was also observed, as previously described, which suggests a redistribution of lymphocytes from the blood to extravascular sites and a mobilization of neutrophils to the peripheral circulation. Further analysis of PBMCs for the frequencies of major T-cell subsets,

Table 1. Blood and Serum Chemistry of Healthy Uninfected RM ($N=2$) After a Single Intravenous Dose of 3 mg/kg PAP-1[a]

	Time						
	RHg7			RVe7			
	0 hrs	48 hrs	7 days	0 hrs	48 hrs	7 days	Reference range
Glucose (mg/dl)	81	94	76	88	122	78	46–178
Urea nitrogen (mg/dl)	13	15	7	16	4	22	8–20
Creatinine (mg/dl)	1.1	0.9	1	1	0.9	0.9	0.8–2.3
Total protein (g/dl)	7.4	7.1	7.5	7.3	7.3	7.2	4.9–9.3
Albumin (g/dl)	4.2	4.1	4.1	4	4	3.8	2.8–5.2
Total bilirubin (mg/dl)	0.2	0.1	0.3	0.1	0.1	0.2	0.1–2.0
Alkaline phosphatase (U/l)	199	206	214	130	138	117	110–966
ALT (U/l)	35	60	30	31	50	27	0–68
AST (U/l)	26	63	27	20	53	24	16–97
Cholesterol (U/l)	97	104	100	136	140	127	108–263
Calcium (mg/dl)	10.3	9	9.8	10.1	9.7	9.9	6.9–13
Phosphorus (mg/dl)	5.1	5.7	4.2	5.1	4.4	5.4	3.1–7.1
Sodium (mEq/l)	139	142	144	139	141	145	102–166
Potassium (mEq/l)	4.4	4.1	4.1	4.0	3.9	4	2.3–6.7
Chloride (mEq/l)	104	104	107	104	105	108	84–126
A/G	1.3	1.4	1.2	1.2	1.2	1.1	—
BUN/creatinine	12	17	7	16	4	24	14–45
Globulin (g/dl)	3.2	3	3.4	3.3	3.3	3.4	2.1–4.1
Lipase (U/l)	29	31	17	18	93	3	12–109
Amylase (U/l)	255	236	243	298	396	275	262–511
Triglycerides (mg/dl)	151	155	125	206	89	132	28–108
CPK (U/l)	134	2734	452	79	1782	1377	—
GGTP (U/l)	44	44	48	57	49	59	—
Magnesium (mEq/l)	1.5	1.4	1.6	1.4	1.3	1.5	—
Calculated osmolality (mOsm/l)	276	282	282	277	278	289	—

[a] RM, rhesus macaques; PAP-1, 5-(4-phenoxybutoxy)psoralen; ALT, alanine aminotransferase; AST, aspartate aminotransferase; A/G, albumin/globulin ratio; BUN, blood urea nitrogen; CPK, creatine phosphokinase; GGTP, gamma-glutamyl transpeptidase.

including $CD4^+$ and $CD8^+$ naive cells, TCMs, TEMs, and $CD4^+$ Tregs, by flow cytometry also reflected this decrease in lymphocytes at the 8-hr time point (Table 2). However, the levels of circulating lymphocytes and serum analytes returned to values near baseline within a week (Tables 1 and 2).

The PK of intravenously administered PAP-1 was also examined in each of the two animals. Plasma samples were collected before and at a number of time points (15 mins, 30 mins, 1 hr, 2 hrs, 4 hrs, 8 hrs, 24 hrs, 48 hrs and 7 days) after PAP-1 administration. PAP-1 plasma concentrations at each time point were determined by HPLC-MS, and the data obtained appeared to be a two-compartment model that followed second-order kinetics (Fig. 4A, left panel). The rate of elimination of PAP-1 was moderately slow, with an *in vivo* half-life of 6.4 hrs. The volume of distribution (Fig 4A, right panel) was between 2–4 l/kg, which is similar to the level previously determined in rats, although the half-life of PAP-1 in these rodents is shorter (3.8 hrs; Ref. 11).

After a washout period of approximately 2 months, and upon confirmation of normal baseline levels of blood/serum chemistry parameters, the safety and efficacy of orally administered PAP-1 (25 mg/kg) was determined in the same two RM. As depicted in Figure 4B, the plasma concentration of PAP-1 peaked within 10 hrs of ingestion and reached a maximum of approximately 1700 n*M* and approximately 950 n*M* in RHg7 and RVe7, respectively. This indicated an efficient absorption of PAP-1 *via* the oral route. There were no signs of toxicity evident in the RM following oral administration of PAP-1. In addition, and similar to the intravenous acute dosing results, fluctuations in serum and hematologic parameters were observed in the 48-hr blood/serum samples after initial ketamine administration, but all values returned to baseline levels within a week (data not shown).

Chronic Dosing of PAP-1 in RM Immunized with the Flu Virus Does Not Appear to Increase Their Susceptibility to Infection and Selectively Inhibits TEM Function but Not the Development of a Central Memory Flu-Specific Response. Because results of the acute dosing studies indicated that there were no detectable toxic side effects at the dose utilized during and following *in vivo* PAP-1 administration, a 30-day chronic-dosing study was initiated in two RM, RGq8 and RWk7. The protocol utilized is outlined in Table 3. The purpose of this experiment was threefold. First, it was necessary to assess the safety of chronic administration of PAP-1 and to determine the dose required to maintain a critical trough

Table 2. Cell Counts of Major Blood Cell Subsets in RM Intravenously Administered 3mg/kg PAP-1[a]

	Time							
	RHg7				RVe7			
	0 hrs	8 hrs	48 hrs	7 days	0 hrs	8 hrs	48 hrs	7 days
Cell counts								
White blood cells (/μl)	5,300	12,200	7,900	4,800	6,800	10,500	10,600	6,300
Red blood cells ($\times 10^6$/μl)	6.08	6.15	5.14	5.18	6.12	6.15	5.38	5.12
Hemoglobin (g/dl)	15.0	15.3	13.1	13.2	15.0	14.7	13.0	12.3
% hematocrit	48.8	48.7	41.3	41.9	49.2	48.4	43.2	41.3
Mean corpuscular volume (fl)	80.3	79.2	80.4	80.9	80.4	78.7	80.3	80.7
MHC (pg)	24.7	24.9	25.5	25.5	24.5	23.9	24.2	24
MHC concentration (g/dl)	30.7	31.4	31.7	31.5	30.5	30.4	30.1	29.8
Platelets ($\times 10^3$/μl)	411	412	354	466	387	411	339	418
Absolute number in blood (/μl)								
Lymphocytes	2,703	732	2,765	2,688	3,190	945	4,346	3,024
$CD4^+$	508	128	495	395	756	222	1117	553
$CD4^+$ naive	119	32	108	79	338	58	454	220
$CD4^+$ central	304	86	283	237	349	148	551	283
$CD4^+$ effector	63	5	81	68	27	6	60	24
$CD8^+$	627	105	807	1,032	1,538	150	1,365	671
$CD8^+$ naive	63	11	50	82	160	12	98	75
$CD8^+$ central	63	21	65	118	124	28	102	60
$CD8^+$ effector	403	55	571	652	1038	88	971	427
$CD4^+/CD8^+$	378	30	373	352	152	28	214	102
$CD4^+/CD8^+$ naive	5	1	4	4	20	3	20	15
$CD4^+/CD8^+$ central	28	7	24	23	31	12	40	22
$CD4^+/CD8^+$ effector	319	22	342	320	90	12	138	58
$CD4^+/CD25^{hi}$	43	11	29	19	73	20	69	55
$CD4^+$/CD25/FoxP3	13	4	9	14	22	8	26	31

[a] RM, rhesus macaques; PAP-1, 5-(4-phenoxybutoxy)psoralen; MHC, mean corpuscular hemoglobin; FOX-P3, forkhead box protein P3.

level of the compound in RM *in vivo*. Second, given that all TEMs and not just antigen-specific TEMs upregulate Kv1.3 channels upon activation, the possibility exists that PAP-1 may globally suppress TEMs and may compromise the host's ability to respond to pathogens. It was therefore critical to ensure that chronic application of PAP-1 does not result in increased susceptibility of the host to opportunistic infection or disease. Finally, the main feature of PAP-1 is that it selectively inhibits the function of TEMs, as shown by previous studies and by the *in vitro* data herein (Fig. 2). It was therefore important to demonstrate that this selectivity holds true *in vivo*.

To accomplish the aforementioned tasks, a chronic dosing study was initiated by administering PAP-1 orally to the two RM daily for a 30-day period at a dosage of 25 mg/kg/day. The oral route was chosen because of logistic limitations of daily intravenous administration, because of the ease of administration, and because pharmacologically relevant levels of PAP-1 were readily detectable in the plasma. The elimination of PAP-1 in RM was previously determined to be relatively slow with a half-life of 6.4 hrs, so the dose was administered once daily. Blood samples were collected at baseline and before each feeding, at the indicated time points (Table 3) and were utilized to determine standard blood/serum chemistry, and served as a source of PBMCs for the analysis of major T-cell subsets by flow cytometry. As seen with the acute-dosing study, chronic oral administration of PAP-1 did not result in any apparent hematologic and organ toxicity, and no marked fluctuations in the frequencies of major T-cell lineages were noted (not shown). Plasma samples were also isolated from the collected blood samples for analysis of PAP-1 concentrations by HPLC-MS. As shown by the results in Table 4, trough levels with concentrations averaging 511 ± 113 n*M* in RGq8 and 77 ± 5 n*M* in RWk7 were maintained throughout the study, which suggested variations in individual uptake levels but also reproducibility within the same individual. After PAP-1 was discontinued, plasma levels decreased according to the established second-order kinetics, and low detectable levels were still present 17 days after PAP-1 was discontinued.

The selective suppressive effect of PAP-1 on TEMs *in vivo* was tested by measuring a potential (but clinically silent) reactivation of cytomegalovirus (CMV) replication by quantifying the levels of CMV DNA in plasma samples from these two RM by real-time PCR. Because CMV levels are believed to be kept in check by TEMs (26, 31), a loss of TEM function was hypothesized to compromise the control of CMV replication. Total viral DNA was isolated from plasma samples of each monkey at various time points

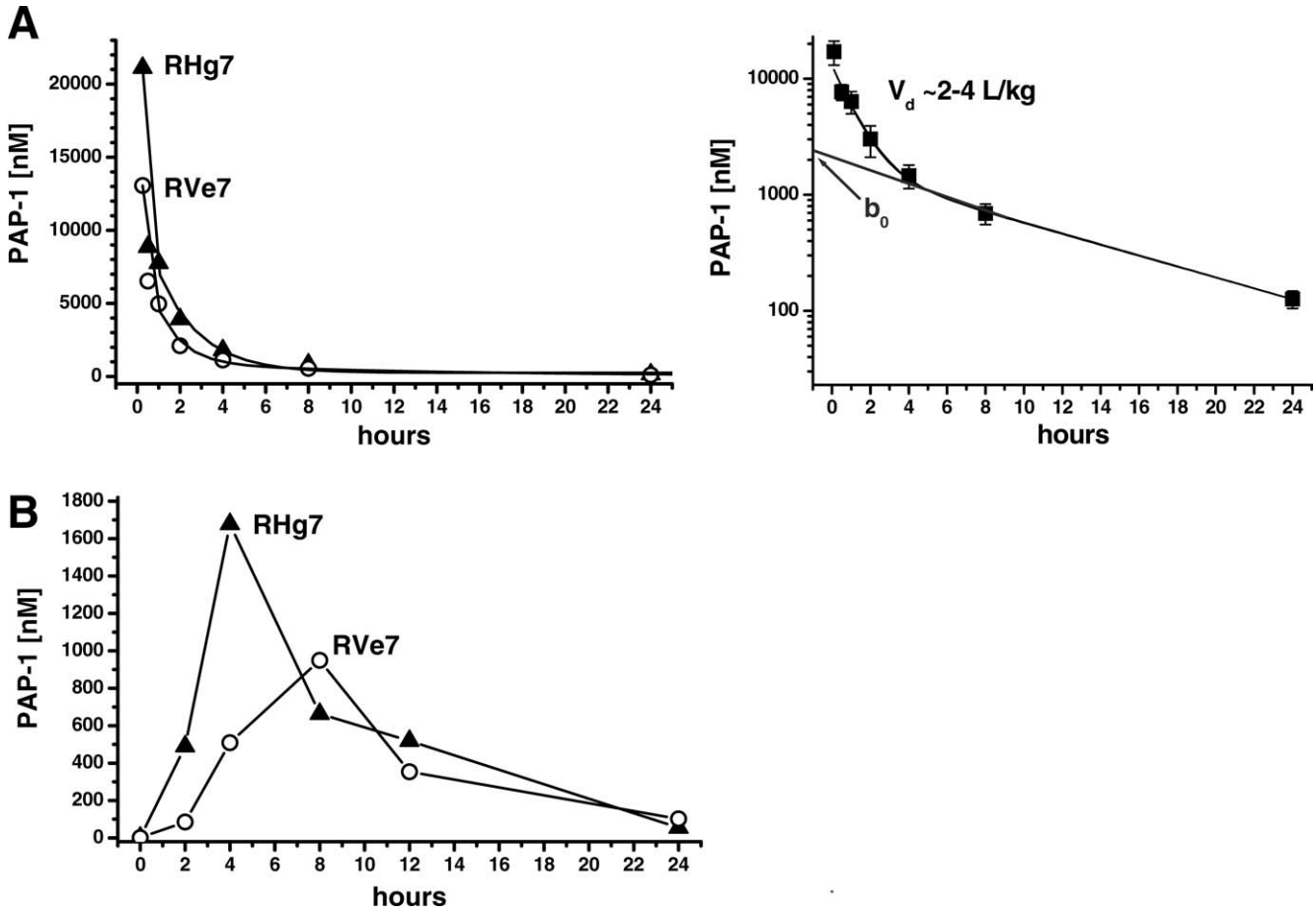

Figure 4. PK of intravenously and orally administered PAP-1 in RM. (A) Total PAP-1 plasma concentration–time profile in RM after single intravenous injection of a 3 mg/kg dose (left) and the log plot of averaged data used to determine the volume of distribution (right). (B) Plasma concentration–time profile in RM that were orally administered 25 mg/kg of PAP-1. Concentrations at 48 hours were 20 n*M* and 30 n*M*; concentrations at 7 days were 10 n*M* and 3 n*M*.

Table 3. PAP-1 Dosing and Flu-Virus Immunization Schedule for RM (RGq8 and RWk7) Undergoing Chronic PAP-1 Treatment[a]

Time point	Dosing/immunization	Measurement
Baseline (0 hrs)	Oral PAP-1 started	Chems/CBC/FACS analysis; ICC + ELISA
12 hrs	—	Chems/CBC/FACS analysis
48 hrs	—	Chems/CBC/FACS analysis
7 days	IN flu virus	Chems/CBC/FACS analysis
14 days	—	Chems/CBC/FACS analysis
21 days	—	Chems/CBC/FACS analysis
28 days	—	Chems/CBC/FACS analysis; flu virus response; ICC + ELISA
30 days	Oral PAP-1 stopped	—
35 days	—	—
37 days	IN flu virus booster	—
47 days	—	Chems /CBC/FACS analysis; flu virus response; ICC + ELISA
93 days	IN flu virus booster	—
103 days	—	Chems/CBC/FACS analysis; Flu virus response; ICC + ELISA

[a] Chems, blood chemistries; CBC, complete blood count; FACS, fluorescence activated cell sorting; IN, intranasal.

Table 4. Plasma Trough Levels of PAP-1 in RM Undergoing the 30-day Chronic Dosing Experiment[a]

	Trough levels (n*M*)	
Time point	RGq8	RWk7
Baseline (0 hrs)	<1.5	<1.5
12 hrs	648	226
48 hrs	344	69
7 days	580	80
14 days	540	77
21 days	582	83
28 days	NA	80
35 days	234	30
47 days	<1.5	1.6

[a] PAP-1, 5-(4-phenoxybutoxy)psoralen; RM, rhesus macaques; NA, sample not available.

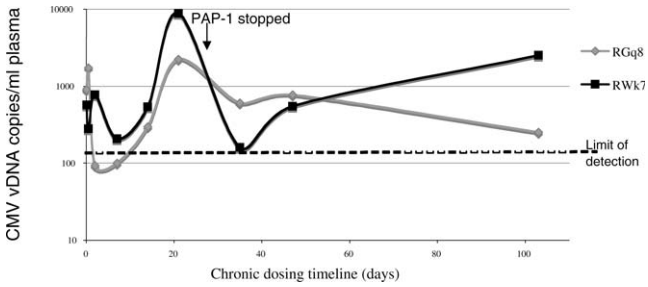

Figure 5. Effect of PAP-1 on plasma CMV levels in RM undergoing chronic PAP-dosing. Real-time PCR was performed to quantify RhCMV levels in viral DNA extracted from plasma samples that were isolated from the two animals before, during and after PAP-1 application. The last day of PAP-1 treatment (Day 30) is indicated.

before, during, and after PAP-1 treatment. Prior to DNA isolation, these plasma samples were also spiked with an equal concentration of a control plasmid, containing the CAT sequence that was later quantified by real-time PCR to ensure consistency in DNA isolation from each sample (data not shown). Quantification of RhCMV revealed that at the baseline time point, both monkeys exhibited detectable, low levels of circulating CMV DNA (approximately 500–1000 copies/ml), which was unexpected (Fig. 5). These RhCMV levels remained relatively near baseline during the first 2 weeks of treatment but an increase did occur as indicated by the peak on Day 21 in both monkeys, with a larger increase being detected in samples from RWk7 (approximately 8800 copies/ml) than from RGq8 (approximately 2200 copies/ml). After PAP-1 was discontinued, RhCMV levels rapidly returned to levels near baseline in both animals.

To further demonstrate the *in vivo* selectivity of PAP-1, both RM were immunized with the flu virus on Day 7, to determine if PAP-1 selectively inhibits the initial flu-specific effector T-cell response but not the development of central memory T-cells. In order to determine the functional nature of the TEM response, the cell-mediated, T-cell immune responses to the flu virus were measured by intracellular cytokine staining (ICC). The frequency of $CD4^+$ and $CD8^+$ T cells that produce the Th1 cytokines IFN-γ, TNF-α, and IL-2 in response to whole-flu virus were determined. As expected, $CD4^+$ and $CD8^+$ T cells from both animals on Day 0 exhibited a minimal response to the OVA peptide (negative control), whereas ConA (positive control) induced a substantial increase in the level of all three cytokines tested (Fig. 6A). Similar control data were observed for samples obtained on Days 28 and 47 (data not shown). In both RM, background levels of flu-specific T-cell responses were observed on Day 28 (3 weeks after the initial flu immunization), indicating that neither animal exhibited a T-cell response while being treated with PAP-1 (Fig. 6B). This was unlike historical controls, in which early flu-specific T-cell responses are clearly evident (32). However, on Day 47, 10 days after the first flu booster and 2 weeks after the discontinuation of PAP-1 treatment, a substantial and significant increase ($P < 0.05$) in the production of IFN-γ and TNF-α by $CD4^+$ T cells (approximately 3% and 2.5% of $CD4^+$ T cells, respectively) was evident in RWk7, the animal which had cleared PAP-1 from the circulation by that time point. Increases in IL-2–producing $CD4^+$ T cells and in cytokine-producing $CD8^+$ T cells were also noted in this animal. Unlike RWk7, only a modest increase in the flu-specific, T-cell response was evident in RGq8 after the first flu booster, which was administered at a time when this animal still had marked levels of PAP-1 present in its system. The cytokine responses in RWk7 and RGq8 were comparable to or greater than those noted for historical controls ($n = 4$) that were not treated with PAP-1 at any time and that exhibited an approximately 2-fold increase in the frequency of IFN-γ–producing $CD4^+$ T cells (1.44% ± 0.35–3.25% ± 0.35) and $CD8^+$ T cells (0.42% ± 0.13–0.98% ± 0.10) following a primary flu booster approximately 46 days after the initial flu immunization (Ansari *et al.*, unpublished data). A second flu booster was administered 2 months later to RWk7 and RGq8, and PBMC samples were analyzed 10 days thereafter. Similar results were obtained, in that a greater flu-specific response was exhibited by RWk7 than by RGq8 (data not shown). Next, the humoral flu-specific immune response in the plasma from these two monkeys was measured using our lab-standardized ELISA. Anti-flu IgG levels in a series of diluted plasma samples from both animals were determined at baseline, at Day 21 (post-initial immunization), at Day 47 (10 days after first booster), and at Day 103 (10 days after second booster). As shown by the antibody titers in Table 5, both animals exhibited a minimal, flu-specific antibody response while undergoing PAP-1 treatment. Similar to the pattern observed with ICC results, a response was only evident in RWk7 and not in RGq8 after the first booster, but both animals exhibited a strong humoral response after the second flu booster, as indicated by the flu antibody titer of 1:10000. As controls, three additional RM were immunized twice with the flu virus but were not administered PAP-1 at any time. Plasma samples were tested for the presence of flu antibody at time points comparable to those of the PAP-1–

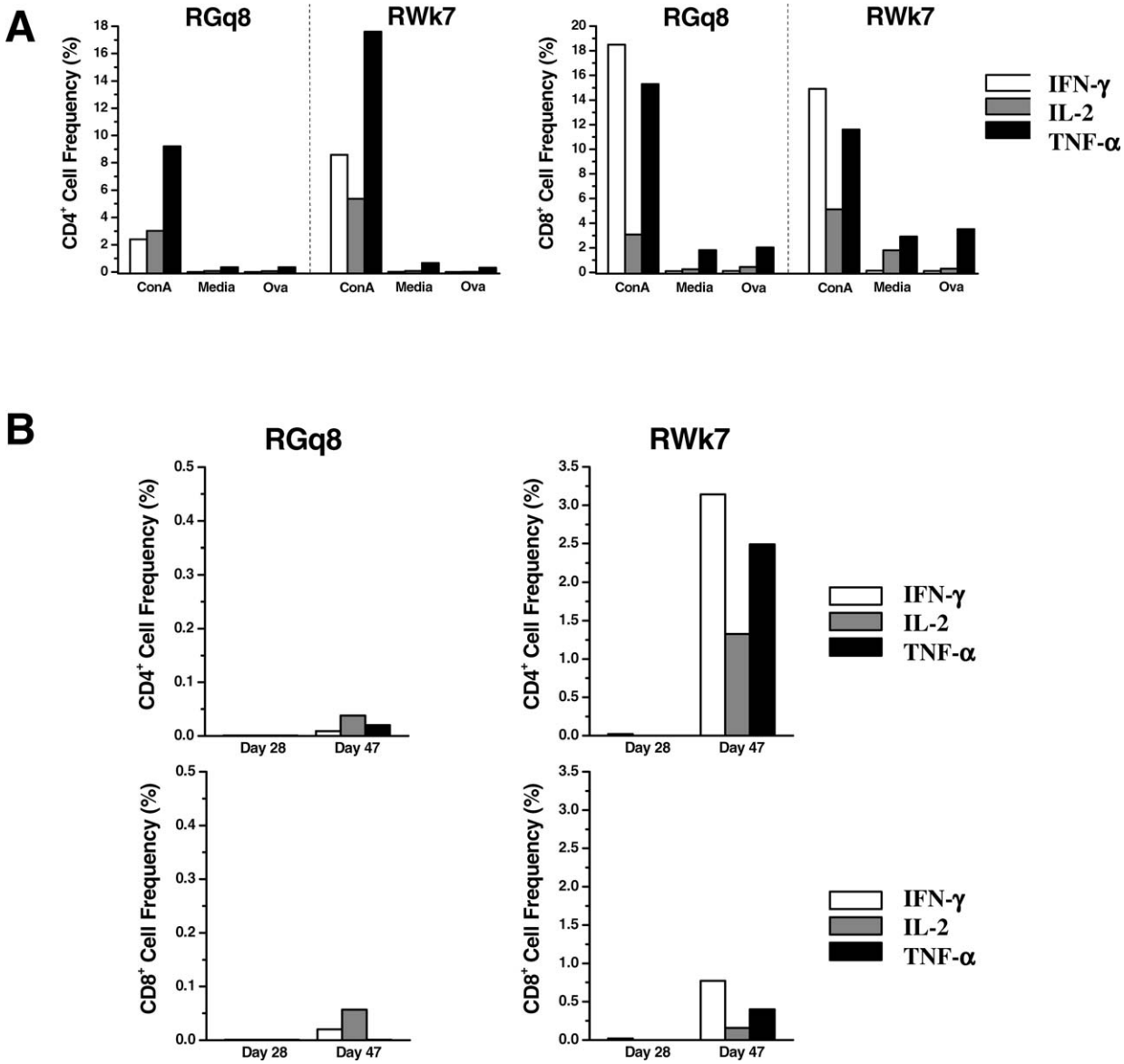

Figure 6. Effect of PAP-1 on the flu virus–specific, primary and secondary T-cell responses in RM. PBMCs that were isolated on Day 28 (during PAP-1 application, after initial flu immunization) and at Day 47 (after PAP-1 application and the first flu booster) were cultured in the presence of ConA (positive control), media (background control), OVA (negative control), and whole-flu virus in the presence of brefeldin A. Cells were surface-stained for CD4 and CD8 and then were fixed/permeabilized and stained to detect IFN-γ (clear bars), IL-2 (dark grey bars), and TNF-α (light grey bars). The frequency of cytokine-producing, $CD4^+$ and $CD8^+$ T cells was determined by flow cytometry. Data shown includes (A) the $CD4^+$ and $CD8^+$ T-cell response to positive (ConA) and negative (media and OVA) controls in both RM on Day 0 (baseline) and (B) the $CD4^+$ and $CD8^+$ T-cell response (corrected for media background) to the flu virus in RGq8 (left panel) and in RWk7 (right panel) on Days 28 and 47.

treated RM. As shown in Table 5, all three control animals exhibited a flu-specific response after the first flu booster, but of particular significance is the fact that a response was already readily detectable in all three control RM 4 weeks after the initial immunization in contrast to the minimal or lack of response in the PAP-1–treated RM. Importantly, neither RGq8 nor RWk7 was adversely affected by the live flu immunization and neither exhibited other signs of disease during the entire course of the PAP-1 chronic dosing experiment.

Discussion

In order to delineate the role of different nonhuman primate lymphoid subset cells in the pathogenesis of SIV infection, our laboratory has been working to identify reagents that can selectively inhibit or deplete certain subsets. Here, we evaluated the toxicity and PK of the recently developed small molecule PAP-1 in RM in order to determine a safe and effective dose for future studies aimed at identifying the role of TEMs in the pathogenesis of SIV infection. PAP-1 and the peptide ShK(L5) have been

Table 5. Flu Antibody Titers in RM Treated or Untreated with PAP-1[a]

		Time point			
		Baseline	3 weeks after flu immunization (Day 28, PAP-1)	10 days after 1st booster (Day 47, no PAP-1)	10 days after 2nd booster (Day 103, no PAP-1)
PAP-1–treated ($n = 2$)	RGq8	<1/100	<1/100	<1/100	1/10,000
	RWk7	<1/100	<1/1,000[b]	1/10,000	1/10,000
		Baseline	4 wks after flu immunization (Day 28, PAP-1)	4 wks after 1st booster (Day 47, no PAP-1)	
Untreated controls ($n = 3$)	RPu3	<1/100	1/1,000	1/1,000	—
	RUq4	<1/100	1/1,000	1/5,000	
	REn4	<1/100	1/1,000	1/1,000	

[a] RM, rhesus macaques; PAP-1, 5-(4-phenoxybutoxy)psoralen.
[b] Borderline negative: mean absorbance = 0.35 versus 0.235 for negative control.

previously shown to preferentially inhibit human and rat TEMs *in vitro* by blocking Kv1.3 in TEMs and to effectively suppress or treat delayed-type hypersensitivity, allergic contact dermatitis, experimental autoimmune encephalomyelitis, pristane-induced arthritis, and type-1 diabetes in rat models (7, 9, 11, 33). Since activated $CD4^+$ TEMs are the primary targets for SIV infection, it was reasoned that the use of PAP-1 in SIV-infected RM would shed light on the role of this important cell lineage in disease progression or resistance. However, prior to conducting such intricate studies in SIV-infected RM, a comprehensive set of *in vitro* and *in vivo* experiments were first performed to determine the safety and efficacy of PAP-1 in healthy RM. PAP-1 had been previously reported to exhibit a 23- to 125-fold selectivity over the closely related Kv1-family channels expressed in the heart (Kv1.5 and Kv1.7) and in neurons and to exhibit a more than 1000-fold selectivity over HERG, sodium, calcium, and chloride channels (7). PAP-1 further did not show any acute or chronic toxicity in rats (33). However, PAP-1 had never before been used in primates, so we needed to determine if it could be safely used in RM. We further needed to ascertain whether RM express high levels of Kv1.3 in activated TEMs, similar to humans and rats (5, 10). This could not simply be assumed, because ion channels often show significant species differences in their expression patterns. For example, besides Kv1.3 and KCa3.1, mouse T cells express Kv1.1, Kv1.2, and Kv1.6 in $CD4^+$ T cells and Kv3.1 in $CD8^+$ T cells; also, they do not upregulate Kv1.3 in TEMs (34–36). Kv1.3 blockers therefore do not inhibit mouse T-cell function *in vitro* (34) and have no effect in mouse autoimmune disease models (37).

Our patch-clamping experiments clearly demonstrated that the potassium channels in T cells of RM are Kv1.3 and KCa3.1. Importantly, of these two channels, Kv1.3 was the one selectively upregulated in activated TEMs, whereas KCa3.1 expression was instead increased in activated naive cells and in TCMs. These findings are in agreement with previous studies involving human T cells (5), thus providing the opportunity to selectively manipulate the function of the TEM subset that uses the Kv1.3-channel blocker PAP-1. This compound and the alternative Kv1.3-specific peptide blocker Shk(L5) were shown to inhibit the Kv1.3 current in activated TEMs and in resting naive T cells, respectively, which may at first suggest that Kv1.3-specific blockers inhibit the function of all T-cell subsets. However, although Kv1.3 channels dominate in all resting T-cell subsets, KCa3.1 channels are rapidly upregulated in naive cells and in TCMs upon activation. As such, these cells are no longer susceptible to Kv1.3 blockade while the TEM subset remains sensitive to its effects. Additional results from *in vitro* suppression assays showed that, although PAP-1 does suppress the proliferation of bulk PBMCs ($IC_{50} = 1\ \mu M$) in RM, the inhibitory effect on CD28-depleted cells was clearly more potent, as indicated by the IC_{50} of 100 n*M*, which is approximately 10-fold higher than that previously reported for human TEMs (10 n*M*; Ref. 7). Since the assay in the previous study by Schmitz *et al.* (7) had utilized purified effector memory T cells and not PBMCs depleted of naive cells and TCMs, the effect of PAP-1 on isolated, CD28-depleted T cells in RM (as opposed to CD28-depleted PBMCs) was also evaluated to determine if this was the cause of the difference. The IC_{50} was approximately 350 n*M* (data not shown), which is greater than that initially obtained for the CD28-depleted PBMC fraction. This is not unexpected because a given number of purified TEMs would require a greater concentration of PAP-1 to be suppressed to the same extent as an equivalent number of the CD28-depleted PBMC fraction that would contain comparatively fewer TEMs. An *in vivo* setting is likely best reflected by the PBMC fraction. Regardless, the *in vitro* IC_{50} of PAP-1 for TEMs of RM is still greater than that for isolated human TEMs. The reason for this difference remains unclear but given that the CD28-depleted cell fraction utilized in the assay was greater than 90% pure, purity issues are highly unlikely and intrinsic differences

between TEMs in RM and in humans possibly contributed to the observed variation in the response to PAP-1. It is also possible that differences in the stimulus used in the previous and current study contributed to these dissimilarities. Nonetheless, the trend is importantly still maintained, with PAP-1 exerting a more potent suppressive effect on TEMs than on naive cells and TCMs in RM.

The Kv1.3-channel expression pattern on TEMs in RM and the *in vitro* selectivity of PAP-1 for this T-cell subset provided a logical basis for pursuing *in vivo* studies. Upon confirmation of the safety and PK of PAP-1, a chronic dosing study was initiated and the moderately long half-life of 6.4 hrs allowed a trough level to be maintained with a single daily dose of 25 mg/kg. Although the trough levels achieved were considerably different in the two RM that were chronically administered PAP-1 (511 n*M* vs. 77 n*M*), these values are still within the normal range of physiologic variability (5×) because of individual differences in absorption and/or rates of metabolism. Importantly, these trough levels indicate that *in vivo* non-toxic plasma concentrations of PAP-1 were achieved and were maintained near or greater than the level that was suppressive for TEMs in RM *in vitro*.

In addition to determining trough levels, the main purpose of the PAP-1 chronic dosing study was to demonstrate that PAP-1 selectively suppresses TEMs *in vivo*. Given that PAP-1 suppresses all TEMs and not only those specific for a particular antigen, it was also crucial to show that the suppression of this T-cell subset would not increase the host susceptibility to opportunistic infection and disease. This was especially important, because RM are carriers of CMV and reactivation of CMV replication due to an immunocompromised system has been documented and may lead to a serious illness (38–42). Quantification of CMV DNA levels by real-time PCR in plasma samples from the two RM before and during chronic PAP-1 treatment indicated a detectable but low level of CMV in both animals even at baseline, which was unexpected. Elevated stress levels associated with repeated access to these RM for previous experiments and those conducted during the recent studies may be a contributing factor to this observation and may also be the reason for the fluctuations observed in CMV DNA levels during the early phase of PAP-1 application. A control of CMV replication was compromised as indicated by the rise in CMV DNA by Day 21. However, the observed increase in CMV DNA copies appears well below the levels reportedly associated with CMV-related illness in RM (43). In a recent study, RM that were undergoing renal allotransplantation and that were administered large boluses of immunosuppressive drugs showed a 1-log–2-log increase in CMV titers without any signs of clinical disease (43). Thus, the modest rise in CMV titers seen in our present study should only be considered a marker of reactivation and not a clinically significant event. Importantly, CMV DNA copy number decreased to levels near baseline following the discontinuation of PAP-1 treatment and no signs of illness were evident throughout the entire course of the study. These data therefore lend support to the selective suppressive effect of PAP-1 on TEMs *in vivo* because this T-cell subset has been described as largely responsibly for the control of CMV replication (26, 31). The results also highlight the need for caution when pursuing a long-term dosing regimen because the extent of CMV reactivation needs to be taken into account.

In addition to the selective inhibitory effect of PAP-1 on TEMs, it was also important to demonstrate that the development or function of the central memory arm was not affected by PAP-1 *in vivo*. To achieve this, both RM were intranasally administered live, attenuated flu virus during PAP-1 treatment and the primary effector and secondary memory cell–mediated and humoral responses were compared before and after PAP-1 application was discontinued. Under normal circumstances of antigenic stimulation, the primary immune response typically involves the activation of naive cells that proliferate to produce cells that are at various stages of differentiation (18, 19). Cells that are at a more terminally differentiated stage exert effector function, whereas those that are at an intermediate level of differentiation persist as TCMs after antigen clearance. Thus, following the initial flu immunization, naive cells will develop into flu-specific TEMs, but their further proliferation and function are expected to be inhibited by PAP-1 while the generation of TCMs should not be affected. Indeed, flow cytometric analyses that were performed 1, 2, and 3 weeks after immunization revealed a modest increase in TEM frequency in both RM (data not shown), and ICC assays also indicated no increase in the production of IFN-γ, IL-2, or TNF-α from $CD4^+$ and $CD8^+$ T cells in response to the flu virus (Fig. 6B; Day 28), which suggests a suppression of the primary effector T-cell response. After PAP-1 was discontinued, two flu boosters were administered to both RM to determine if the generation of central memory cells was affected by PAP-1. ICC data indicated that a stronger memory T cell response was exhibited by RWk7 than by RGq8. These cytokine responses were readily detectable and were comparable to or greater than those exhibited by historical controls that were also administered the flu virus but not treated with PAP-1. This suggests that a functional, secondary, flu-specific memory response was maintained and was exhibited by the PAP-1–treated RM. Similarly, results from the ELISA showed a lack of flu-specific IgG production in the PAP-1–treated RM 3 weeks after the initial immunization, in contrast to the untreated RM, which clearly exhibited an antibody response. However, both PAP-1–treated RM exhibited a flu-specific IgG response after administration of a second flu booster, which suggests that the generation of central memory B cells was not affected. The secondary IgG response exhibited by RGq8 was again weaker than that of RWk7. Since RGq8 had maintained approximately 7-fold greater trough levels of PAP-1 than RWk7 (Table 4), it is tempting to speculate that this may have been the reason for

the minimal flu-specific response in this monkey. However, the response of a larger cohort of animals to PAP-1, including the parallel use of *bona fide* controls would need to be examined in order to derive a definite correlation between *in vivo* PAP-1 plasma concentrations and the suppression of antigen-specific immune responses.

The fact that the IgG responses were also influenced by PAP-1 raises the important point that PAP-1 affects not only a single cell subset (i.e., TEMs) but in fact also has an impact on B cells. Indeed, PAP-1 has been previously shown to inhibit the proliferation and function of class-switched $IgD^{-}CD27^{+}$ B cells but not activated naive and $IgD^{+}CD27^{+}$ B cells (6). This in combination with the suppressive effect of PAP-1 on $CD4^{+}$ TEMs with Th2 function may have contributed to the inhibition of the primary B-cell mediated IgG response. One may then posit how an IgG response was generated after the flu booster, given that PAP-1 should have suppressed memory class–switched B cells. Because PAP-1 does not affect the generation of $IgD^{+}CD27^{+}$ memory cells, it is possible that this compartment was able to undergo class switching after the booster immunizations. It would be of interest to evaluate the nature of the antibody response elicited when RM are immunized with flu boosters while still being administered PAP-1 to determine if antibody production would be limited to only IgM and not to IgG. These observations therefore stress the need for caution when interpreting results from the PAP-1 chronic dosing study, because its effect is exerted on not only a single cell subset but in fact influences both the cell-mediated and humoral arms of the immune system. It is also important to bear in mind that the nature and level of Kv1.3 expression in other major cell subsets, such as natural killer cells/natural killer T cells, has not been elucidated, although it has been suggested that components of the innate immune system are unaffected by Kv1.3 blockade (44). A recent study demonstrated the presence of both Kv1.3 and Kv1.5 channels on human peripheral dendritic cells, which suggests that PAP-1 may also influence the function of this cell subset. However, the presence of the alternate potassium channel Kv1.5 may offset any inhibitory effect caused by PAP-1. The potential inhibitory effect of PAP-1 on other major cell lineages therefore remains to be clarified and the influence of this on disease outcome cannot be overlooked. However, worthy of mention is that the two RM that were undergoing chronic dosing of PAP-1 were not adversely affected by the live flu virus that normally replicates only in the upper respiratory tract and occasionally produces mild symptoms, such as transient nasal discharge, in healthy monkeys. Of note, such symptoms were not observed throughout the entire course of the study. Thus, the immune systems of the two RM in the study were not significantly compromised by PAP-1, at least during the short-term chronic dosing regimen.

In summary, the results from this study collectively show that the utilization of PAP-1 in RM is both safe and effective, which opens the door for PAP-1 use in SIV-infected RM to determine the effect of this small molecule on major cell lineages and to define those that play a major role in SIV pathogenesis. Future studies would therefore include administering PAP-1 to SIV-infected RM during the acute or chronic phase of infection to determine if the inhibition of TEM function prevents or slows disease progression to AIDS by limiting the number of viral cell targets and/or by muting the chronic immune hyperactivation exhibited by SIV-infected RM. Although the utilization of PAP-1 in an SIV-infected RM model particularly during the acute phase of infection may potentially limit the pool of viral target cells by inhibiting $CD4^{+}$ TEM function and proliferation, the effect on $CD8^{+}$ TEMs that assist in VL control cannot be overlooked. It is possible that, if a lower VL setting is achieved because of inhibition of $CD4^{+}$ TEMs, other cell lineages implicated in immune control, such as NK cells and B cells, may contribute to VL control, possibly bypassing the need for a rigorous $CD8^{+}$ TEM response. Because the effects of PAP-1 are almost immediately reversible, any detrimental effects on VL control can be relieved by discontinuing treatment or by lowering the dose. One may also test if the PAP-1 dose can be titrated to a concentration that perhaps maintains a balance between $CD4^{+}$ TEM inhibition and $CD8^{+}$ TEM function. In addition to the application of PAP-1 in RM, its use can also be applied in SIV-infected sooty mangabeys (SM), nonhuman primates that remain disease-free throughout the course of SIV infection (13, 45, 46). The aim would be to determine the cause of disease resistance in this species and to evaluate if the inhibition of TEM function in SM results in disease development. Preliminary *in vitro* experiments performed by us have shown that the Kv1.3-channel expression pattern in T cells of SM is very similar to that of T cells in RM and of human T cells. In addition, PAP-1 inhibits the Kv1.3 current, as shown by patch-clamping experiments, and it also effectively suppresses the proliferation of both PBMCs and isolated TEM cells from SM *in vitro* (data not shown). The potential application for the use of PAP-1 in this nonhuman primate is therefore a reality, and these studies together with those involving RM are sure to further our understanding of the mechanisms involved in disease resistance and susceptibility in SIV-infected hosts. The observed differential expression of KCa3.1 channels in RM T-cells (Fig. 2) and in T cells of SM (not shown) and the availability of the KCa3.1-specific blocker TRAM-34 (8) provide the opportunity to manipulate naive cells and central, memory cell subsets, which may prove to be beneficial during acute stages of infection. Further studies involving this additional potassium channel blocker therefore are warranted.

We thank Daniel Homerick for excellent technical assistance with the HPLC-MS assay, Dr. K. George Chandy for helpful suggestions with the study, and the Yerkes National Primate Research staff for their excellent care of the animals and sample collections.

1. Chandy KG, Wulff H, Beeton C, Pennington M, Gutman GA, Cahalan MD. K+ channels as targets for specific immunomodulation. Trends Pharmacol Sci 25:280–289, 2004.
2. Freedman BD, Price MA, Deutsch CJ. Evidence for voltage modulation of IL-2 production in mitogen-stimulated human peripheral blood lymphocytes J Immunol 149:3784–3794, 1992.
3. Leonard RJ, Garcia ML, Slaughter RS, Reuben JP. Selective blockers of voltage-gated K+ channel depolarize human T lymphocytes: mechanism of the antiproliferative effect of charybdotoxin. Proc Natl Acad Sci U S A 89:10094–10098, 1992.
4. Lin CS, Boltz RC, Blake JT, Nguyen M, Talento A, Fischer PA, Springer MS, Sigal NH, Slaughter RS, Garcia ML, Kaczorowski GJ, Koo GC. Voltage-gated potassium channels regulate calcium-dependent pathways involved in human T lymphocyte activation. J Exp Med 177:637–645, 1993.
5. Wulff H, Calabresi PA, Allie R, Yun S, Pennington M, Beeton C, Chandy KG. The voltage-gated Kv1.3 K+ channel in effector memory T cells as a new target for MS. J Clin Invest 111:1703–1713, 2003.
6. Wulff H, Knaus H-G, Pennington M, Chandy KG. K+ channel expression during B cell differentiation: implications for immunomodulation and autoimmunity. J Immunol 173:776–786, 2004.
7. Schmitz A, Sankaranarayanan A, Azam P, Schmidt-Lassen K, Homerick D, Hansel W, Wulff H. Design of PAP-1, a selective small molecule Kv1.3 blocker, for the suppression of effector memory T cells in autoimmune diseases. Mol Pharmacol 68:1254–1270, 2005.
8. Wulff H, Miller MJ, Hansel W, Grissmer S, Cahalan MD, Chandy KG. Design of a potent and selective inhibitor of the intermediate-conductance Ca2+-activate K+ channel, IKCa1: a potential immunosuppressant. Proc Natl Acad Sci U S A 97:8151–8156, 2000.
9. Beeton C, Pennington MW, Wulff H, Singh S, Nugent D, Crossley G, Khaytin I, Calabresi PA, Chen CY, Gutman GA, Chandy KG. Targeting effector memory T cells with a selective peptide inhibitor of Kv1.3 channels for therapy of autoimmune diseases. Mol Pharmacol 67:1369–1381, 2005.
10. Beeton C, Wulff H, Barbaria J, Clot-Faybesse O, Pennington M, Bernard D, Cahalan MD, Chandy KG, Beraud E. Selective blockade of T lymphocyte K+ channels ameliorates experimental autoimmune encephalomyelitis, a model for multiple sclerosis. Proc Natl Acad Sci U S A 98:13942–13947, 2001.
11. Beeton C, Wulff H, Standifer NE, Azam P, Mullen KM, Pennington MW, Kolski-Andreaco A, Wei E, Grino A, Counts DR, Wang PH, LeeHealey CJ, Andrews BS, Sankaranarayanan A, Homerick D, Roeck WW, Tehranzadeh J, Stanhope KL, Zimin P, Havel PJ, Griffey S, Knaus H-G, Nepom GT, Gutman GA, Calabresi PA, Chandy KG. Kv1.3 channels are a therapeutic target for T cell-mediated autoimmune diseases. Proc Natl Acad Sci U S A 103:17414–17419, 2006.
12. Firpo PP, Axberg I, Scheibel M, Clark EA. Macaque CD4+ T-cell subsets: influence of activation on infection by simian immunodeficiency viruses (SIV). AIDS Res Hum Retroviruses 8:357–366, 1992.
13. Kaur A, Grant RM, Means RE, McClure H, Feinberg M, Johnson RP. Diverse host responses and outcomes following simian immunodeficiency virus SIVmac239 infection in sooty mangabeys and rhesus macaques. J Virol 72:9597–9611, 1998.
14. Veazey RS, Tham IC, Mansfield KG, DeMaria M, Forand AE, Shvetz DE, Chalifoux LV, Sehgal PK, Lackner AA. Identifying the target cell in primary simian immunodeficiency virus (SIV) infection: highly activated memory CD4(+) T cells are rapidly eliminated in early SIV infection in vivo. J Virol 74:57–64, 2000.
15. Finzi D, Hermankova M, Pierson T, Carruth LM, Buck C, Chaisson RE, Quinn TC, Chadwick K, Margolick J, Brookmeyer R, Gallant J, Markowitz M, Ho DD, Richman DD, Siliciano RF. Identification of a reservoir for HIV-1 in patients on highly active antiretroviral therapy. Science 278:1295–1300, 1997.
16. Finzi D, Siliciano RF. Viral dynamics in HIV-1 infection. Cell 93: 6314–6319, 1998.
17. Hazenberg MD, Otto SA, Benthem BHV, Roos MT, Coutinho RA, Lange JM, Hamann D, Prins M, Miedema F. Persistent immune activation in HIV-1 infection is associated with progression to AIDS. AIDS 17:1881–1888, 2003.
18. Sallusto F, Geginat J, Lanzavecchia A. Central memory and effector memory T cell subsets: Function, Generation, and Maintenance. Ann Rev Immunol 22:745–763, 2004.
19. Song K, Rabin RL, Hill BJ, Rosa SCD, Perfetto SP, Zhang HH, Foley JF, Reiner JS, Liu J, Mattapallil JJ, Douek DC, Roederer M, Farber JM. Characterization of subsets of Cd4+ memory T cells reveals early branched pathways of T cell differentiation in humans. Proc Natl Acad Sci U S A 102:7916–7921, 2005.
20. Kuroda MJ, Schmitz JE, Charini WA, Nickerson CE, Lifton MA, Lord CI, Forman MA, Letvin NL. Emergence of CTL coincides with clearance of virus during primary simian immunodeficiency virus infection in rhesus monkeys. J Immunol 162:5127–5133, 1999.
21. National Research Council. Guide for the care and use of laboratory animals. Washington DC: National Academic Press, 1996.
22. Ansari AA, Bostik P, Mayne AE, Villinger F. Failure to expand influenza and tetanus toxoid memory T cells in vitro correlates with disease course in SIV infected rhesus macaques. Cell Immunol 210: 125–142, 2001.
23. Pitcher CJ, Hagen SI, Walker JM, Lum R, Mitchell BL, Maino VC, Axthelm MK, Picker LJ. Development and homeostasis of T cell memory in rhesus macaque. J Immunol 168:29–43, 2002.
24. Knuchel M, Bednarik DP, Chikkala N, Ansari AA. Biphasic in vitro regulation of retroviral replication by CD8+ cells from nonhuman primates J Acquir Immune Defic Syndr 7:438–446, 1994.
25. Knuchel M, Bednarik DP, Chikkala N, Villinger F, Folks TM, Ansari AA. Development of a novel quantitative assay for the measurement of chloramphenicol acetyl transferase (CAT) mRNA. J Virol Methods 48: 325–338, 1994.
26. Kaur A, Hale CL, Noren B, Kassis N, Simon MA, Johnson RP. Decreased frequency of cytomegalovirus (CMV)-specific CD4+ T lymphocytes in simian immunodeficiency virus-infected rhesus macaques: inverse relationship with CMV viremia. J Virol 76:3646–3658, 2002.
27. Grissmer S, Dethlefs B, Wasmuth JJ, Goldin AL, Gutman GA, Cahalan MD, Chandy KG. Expression and chromosomal localization of a lymphocyte K+ channel gene. Proc Natl Acad Sci U S A 87:9411–9415, 1990.
28. Sallusto F, Lenig D, Forster R, Lipp M, Lanzavecchia A. Two subsets of memory T lymphocytes with distinct homing potentials and effector functions. Nature 401:708–712, 1999.
29. Bennett JS, Gossett KA, McCarthy MP, Simpson ED. Effects of ketamine hydrochloride on serum biological and hematological variables in rhesus monkeys (Macaca mulatta). Vet Clin Pathol 21: 15–18, 1992.
30. Kim C-Y, Lee H-S, Han S-C, Heo J-D, Kwon M-S, Ha C-S, Han S-S. Hematological and serum biochemical values in cynomologus monkeys anesthesized with ketamine hydrochloride. J Med Primatol 34:96–100, 2005.
31. Kaur A, Daniel MD, Hempel D, Martin D, Hirsch S, Johnson RP. Cytotoxic T-Lymphocyte Responses to Cytomegalovirus Normal and Simian Immunodeficiency Virus-Rhesus Macaques. J Virol 70:7725–7733, 1996.
32. Villinger F, Brice GT, Mayne AE, Bostik P, Mori K, June CH, Ansari AA. Adoptive transfer of simian immunodeficiency virus (SIV) naive autologous CD4+ cells to macaques chronically infected with SIV is sufficient to induce long-term nonprogressor status. Blood 99:590–599, 2002.
33. Azam P, Sankaranarayanan A, Homerick D, Griffey S, Wulff H. Targeting effector memory T cells with the small molecule Kv1.3

blocker PAP-1 suppresses allergic contact dermatitis. J Invest Dermatol 127:1419–1429, 2007.

34. Freedman BD, Fleischmann BK, Punt J, Hashimoto Y, Gaulton G, Kotlikoff MI. Identification of Kv1.1 expression by murine CD4-CD8- thymocytes: A role for voltage-dependent K + channels in murine thymocyte development. J Biol Chem 270:22406–22411, 1995.
35. Lewis RS, Cahalan MD. Subset-specific expression of potassium channels in developing murine T lymphocytes. Science 239:771–775, 1988.
36. Beeton C, Chandy KG. Potassium channels, memory T cells, and multiple sclerosis. Neuroscientist 11:550–562, 2005.
37. Koo GC, Blake JT, Talento A, Nguyen M, Lin S, Sirotina A, Shah K, Mulvany K, Jr DH, Cunningham P, Wunderler DL, McManus OB, Slaughter R, Bugianesi R, Felix J, Garcia M, Williamson J, Kaczorowski G, Sigal NH, Springer MS, Feeney W. Blockade of the voltage-gated potassium channel Kv1.3 inhibits immune responses in vivo. J Immunol 158:5120–5128, 1997.
38. Asher DM, Jr CJG, Lang DJ, Gajdusek DC. Persistent shedding of cytomegalovirus in the urine of healthy monkeys (37897). Proc Soc Exp Biol Med 145:794–801, 1974.
39. Baskin GB. Disseminated cytomegalovirus infection in immunodeficient rhesus monkeys. Am J Pathol 129:345–352, 1987.
40. Osborn KG, Prahalada S, Lowenstine LJ, Gardner MB, Maul DH, Henrickson RV. The pathology of an epizootic of acquired immunodeficiency in in rhesus macaques. Am J Pathol 114:94–103, 1984.
41. Vogel P, Weigler BJ, Kerr H, Hendrickx AG, Barry PA. Seroepidemiologic studies of cytomegalovirus infection in a breeding population of rhesus macaques. Lab Anim Sci 44:25–30, 1994.
42. Kaur A, Kassis N, Hale CL, Simon M, Elliott M, Gomez-Yafal A, Lifson JD, Desrosiers RC, Wang F, Barry P, Mach M, Johnson RP. Direct relationship between suppression of virus-specific immunity and emergence of cytomelgalovirus disease in simian AIDS. J Virol 77: 5749–5758, 2003.
43. Kean LS, Adams AB, Strobert E, Hendrix R, Gangappa S, Jones TR, Shirasugi N, Rigby MR, Hamby K, Jiang J, Bello H, Anderson D, Cardona K, Durham MM, Pearson TC, Larsen CP. Induction of chimerism in rhesus macaques through stem cell transplant and costimulation blockade-based suppression. Am J Transplant 7:320–335, 2007.
44. Shah K, Blake JT, Huang C, Fischer P, Goo GC. Immunosuppressive effects of a Kv1.3 inhibitor. Cell Immunol 221:100–106, 2003.
45. Silvestri G, Fedanov A, Germon S, Kozyr N, Kaiser WJ, Garber DA, McClure H, Feinberg MB, Staprans SI. Divergent host responses during primary simian immunodeficiency virus SIVsm infection of natural sooty mangabey and nonnatural rhesus macaque hosts. J Virol 79:4043–4054, 2005.
46. Silvestri G, Sodora DL, Koup RA, Paiardini M, O'Neil SP, McClure HM, Staprans SI, Feinberg MB. Nonpathogenic SIV infection of sooty mangabeys is characterized by limited bystander immunopathology despite chronic high-level viremia. Immunity 18:441–452, 2003.